A micromechanical model of a hard interface with micro-cracking damage

Maria Letizia Raffa, Frédéric Lebon, Raffaella Rizzoni

A micromechanical model of a hard interface with micro-cracking damage

Maria Letizia Raffa[a,*], Frédéric Lebon[b], Raffaella Rizzoni[c]

[a] *Laboratoire QUARTZ, EA 7393, ISAE-Supméca, 3 rue Fernand Hainaut 93407 Saint-Ouen, France*
[b] *Aix Marseille Univ, CNRS, Centrale Marseille, LMA, 4 impasse Nikola Tesla 13453 Marseille Cedex 13, France*
[c] *Department of Engineering, University of Ferrara, via Saragat 1 44122 Ferrara, Italy*

Abstract

Bonding techniques are increasingly used in many industrial fields. Modelling the under-load damaging behavior of hard structural adhesives is still an open challenge. This work proposes a new hard interface analytical model with evolutive micro-cracking damage. The model is obtained within a rigorous theoretical framework combining asymptotic theory and micromechanical homogenization. Main new features are: (i) the adoption of two dual homogenization approaches; (ii) the formulation of a thermodynamically-based damage evolution law for hard interfaces. The interface model is able to describe both ductile and brittle damage behavior of hard structural adhesives. Provided examples on the structural behavior, under several loads, suggest the suitability of the proposed interface model as a modelling strategy for hard structural adhesives with micro-cracking damage.

*Corresponding author

Email addresses: maria-letizia.raffa@isae-supmeca.fr (Maria Letizia Raffa), lebon@lma.cnrs-mrs.fr (Frédéric Lebon), raffaella.rizzoni@unife.it (Raffaella Rizzoni)

Keywords: bonding, adhesives, damage, imperfect interfaces, homogenization, asymptotic theory

1. Introduction

Bonding has become a very common practice to assembly materials and structural elements in many industrial fields, such as aeronautic, spatial, automotive, nuclear, civil, mechanical and bio-engineering, mainly because structural adhesives offer low-cost techniques and a great design freedom while preserving good mechanical performances. For some applications, such as assemblies of fiber-reinforced composites and implant fixations, bonding is the only viable assembly technology. To achieve better performances avoiding too large mismatch in terms of thermo-elastic properties, structural adhesives and adherents have, in some cases, an equivalent stiffness. Some examples can be cited: acrylic adhesives, whose Young's modulus (E) is around 2-3 GPa [1], are used in manufacture of plywood ($E = 5 - 8$ GPa); phenolic and epoxy adhesives with $E = 3 - 5$ GPa [2] are used to bond structures of GFRP (polyester-glass composites) with $E = 15 - 28$ GPa; orthodontic adhesives with $E = 18 - 22$ GPa [3] are usually used for cementation of brackets on enamel ($E \simeq 65$ GPa).

An adhesive equally stiffer than adherents is defined, from a mechanical point of view, as a *hard* interface, as opposed to the definition of *soft* interface [4, 5]. A wide literature exists concerning models of soft material interfaces, including those undergoing material degradation. Analytical soft interface models often take into account the nonlinear evolution of the interface properties by introducing at least one parameter (of damage, adhesion, etc.) whose variation depends macroscopically on kinematic variables [6–15]. Numerical soft interface models, in the framework of the finite element theory, generally use cohesive zone models (CZM) based on traction-separation laws of various shapes, to describe cohesive and adhesive failure [16–22].

Recently, some analytical models of hard material interfaces have been also developed [23–29] and it has been proved that interface models developed for soft adhesives cannot be directly applied in the case of hard adhesives [25]. Moreover, the existing hard interface models do not consider the degradation of the adhesive material properties.

This paper provides a novelty within this context, by proposing a hard material interface model accounting for an evolutive micro-cracking damage. In the last twenty years, the present authors established an original modelling strategy to derive soft and hard imperfect interface models based on the combination of asymptotic theory and micromechanical homogenization [11, 14, 23–26] (see Fig. 1). This strategy has already been successfully used to describe the mechanics of thin elastic layers in adhesive-like problems and contact problems [13, 15, 30, 31]. Moreover, it has been identified as a sound alternative to the classical cohesive zone models, principally because imperfect interface models allow to consider the physics of the adhesives in terms of geometrical (thickness, surface roughness), mechanical (anisotropy, non-linearity) and damage properties.

This work is an extension of the authors' modelling strategy of hard imperfect interfaces. Drawing on Kachanov's micromechanical homogenization theory [32–37], micro-cracking damage is represented by a microcracks density parameter. Particularly, the adoption of a generalized cracks density [38]

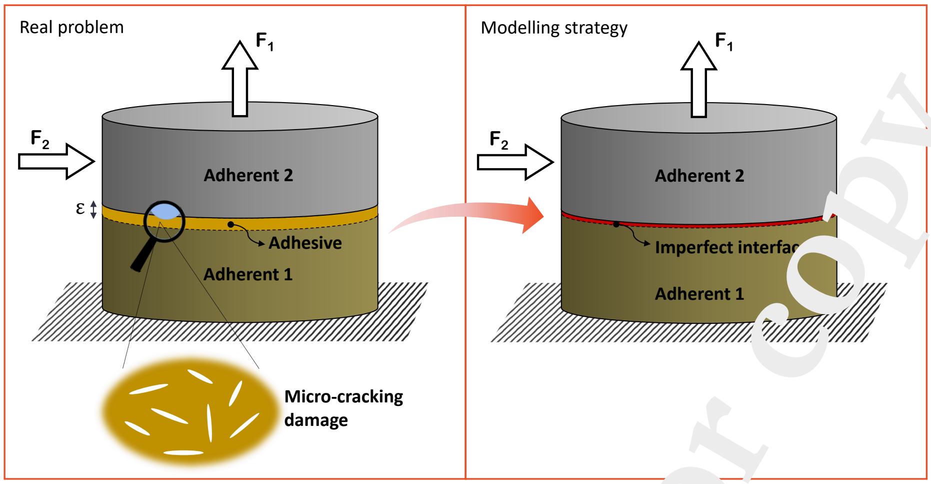

Fig. 1: Schematic sketch of the imperfect interface modelling strategy

allows to by-pass the geometrical definition of the cracks, which is possible only for circular and regular cracks [32], and as a matter of fact it extends the generality of the proposed interface model to any regular and irregular cracks shape. It should also be noted that the generalized microcracks density can be measured *postmortem* by X-ray micro-tomography [15]. The evolutive character of the micro-cracking damage is described by introducing a new evolution law of the generalized cracks density.

The paper is structured as follows. The hard imperfect interface law is derived via the asymptotic expansions method in Section 2. In Section 3, the microcracked-material-interface properties are derived through two dual approaches of micromechanical homogenization, stress [32, 33] and strain-based [39, 40]. The damage evolution law is derived from a thermodynamic approach and then included in the hard interface model via the asymptotic expansions method. In Section 4, the behavior of the proposed interface model under various loading type is discussed via some academic examples. Moreover, the influence of damage parameters is investigated. Conclusions and perspectives are drawn at the end of the paper.

2. Derivation of the hard imperfect interface model

2.1. Notation and problem statement

The herein adopted matched asymptotic expansion theory builds on the tradition of using asymptotic analysis to derive mechanical laws governing imperfect interface conditions [41–48].

In what follows, a thin material layer of constant thickness t embedded between at least two solids is referred as *interphase*. Being L a representative length scale of the geometry, the non-dimensional interphase thickness $\varepsilon = t/L$ can be defined and taken as a small parameter for the asymptotic expansions of the elastic problem. When $\varepsilon \ll 1$, the thin layer can be substituted by a surface separating the adherents called *interface* across which certain conditions on the displacements and tractions prevail [4].

The interphase occupies a domain $\mathcal{B}^{\varepsilon}$ with cross-section $\mathcal{S}$, $\mathcal{S}$ being an open bounded set in $\mathbb{R}^2$ with a smooth boundary. The *adherents* occupy the reference configurations $\Omega^{\varepsilon}{}_{\pm} \subset \mathbb{R}^3$. Let $\mathcal{S}^{\varepsilon}{}_{\pm}$ be taken to denote the plane interfaces between interphase and adherents and let $\Omega^{\varepsilon} = \Omega^{\varepsilon}{}_{\pm} \cup \mathcal{S}^{\varepsilon}{}_{\pm} \cup \mathcal{B}^{\varepsilon}$ denote the whole composite system. It is assumed that the displacement and stress vector fields are continuous across $\mathcal{S}^{\varepsilon}{}_{\pm}$.

An orthonormal Cartesian basis $(O, \mathbf{i}_1, \mathbf{i}_2, \mathbf{i}_3)$ is introduced and let (x_1, x_2, x_3)

be taken to denote the three coordinates of a particle. The origin of the basis belongs to $\mathcal{S}$. The aforementioned system is sketched in Fig. 2a.

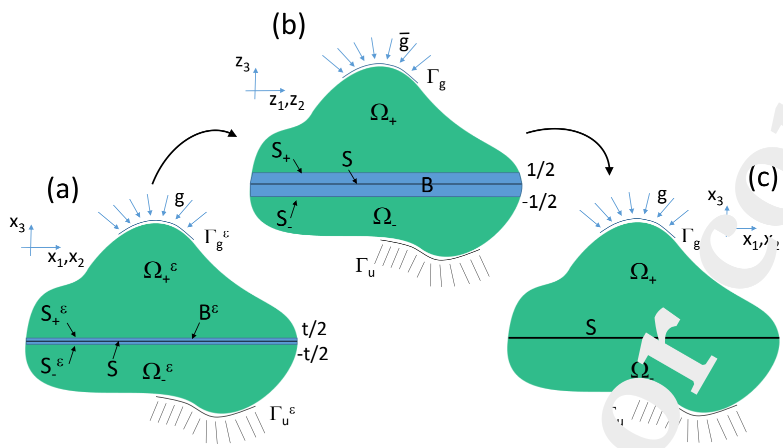

Fig. 2: The three steps of the matched asymptotic expansion method: (a) Reference configuration (interphase); (b) Rescaled configuration (asymptotic expansion phase); (c) Limit configuration (interface).

The materials of the composite system are assumed to be homogeneous and linearly elastic and let $\mathbb{A}_\pm, \mathbb{B}^\varepsilon$ be the fourth-rank elasticity tensors of adherents and of interphase, respectively. Tensors $\mathbb{A}_\pm$, $\mathbb{B}^\varepsilon$ have the usual symmetry properties, with the minor and major symmetries, and are positive definite. Note that any assumption on the anisotropy of adhesive and adherents materials is needed for the proposed development. As a matter of fact, it extends the generality of the proposed asymptotic approach to any anisotropic material.

Adherents are subjected to a body force density $\mathbf{f}^\pm : \Omega^\varepsilon{}_\pm \mapsto \mathbb{R}^3$ and to a surface force density $\mathbf{g}^\pm : \Gamma_g^\varepsilon \mapsto \mathbb{R}^3$ on $\Gamma_g^\varepsilon \subset (\partial\Omega^\varepsilon{}_+ \setminus \mathcal{S}_+^\varepsilon) \cup (\partial\Omega^\varepsilon{}_- \setminus \mathcal{S}_-^\varepsilon)$. Body forces in the interphase are neglected.

On $\Gamma_u^\varepsilon = (\partial\Omega^\varepsilon{}_+ \backslash \mathcal{S}_+^\varepsilon) \cup (\partial\Omega^\varepsilon{}_- \backslash \mathcal{S}_-^\varepsilon) \backslash \Gamma_g^\varepsilon$, homogeneous boundary conditions are prescribed:

$$\mathbf{u}^\varepsilon = \mathbf{0} \quad \text{on } \Gamma_u^\varepsilon, \tag{1}$$

where $\mathbf{u}^\varepsilon : \Omega^\varepsilon \mapsto \mathbb{R}^3$ is the displacement field defined on Ω^ε. Boundaries Γ_g^ε, Γ_u^ε are assumed to be located sufficiently far from the interphase and the external boundaries of the interphase $\mathcal{B}^\varepsilon$ $(\partial\mathcal{S} \times (-\frac{\varepsilon}{2}, \frac{\varepsilon}{2}))$ are assumed to be stress-free. The external forces field is endowed with sufficient regularity to ensure the existence of an equilibrium configuration [25].

The following notation is adopted:

- $[f] := f(\mathbf{z}_\alpha, \frac{1}{2}) - f(\mathbf{z}_\alpha, -\frac{1}{2}) \Rightarrow$ jump in the rescaled configuration (Fig. 2b);
- $\langle f \rangle := \int_{-\frac{1}{2}}^{\frac{1}{2}} f(\mathbf{z}_\alpha, z_3) dz_3 \Rightarrow$ average in the rescaled configuration;
- $[[f]] := f(\mathbf{x}_\alpha, 0^+) - f(\mathbf{x}_\alpha, 0^-) \Rightarrow$ jump in the limit configuration (Fig. 2c);
- $\langle\langle f \rangle\rangle := \frac{1}{2}(f(\mathbf{x}_\alpha, 0^+) + f(\mathbf{x}_\alpha, 0^-)) \Rightarrow$ average in the limit configuration;

where f is a generic function, $\mathbf{z}_\alpha = (z_1, z_2)$ and $\mathbf{x}_\alpha = (x_1, x_2)$.

2.2. The one-order asymptotic theory

This section details the main steps of the asymptotic analysis leading to the hard interface law at one order. Full formulation is reported in Appendix A and more details could be found in [23–26].

Generally, the elasticity tensor $\mathbb{B}^\varepsilon$ of a hard interphase does not depend on ε [23, 25]:

$$\mathbb{B}^\varepsilon = \mathbb{B} \tag{2}$$

In the rescaled configuration (Fig. 2b) and considering Eqs. (A.7) and (A.14b), the stress-strain equation (A.31b) reads as:

$$\hat{\boldsymbol{\sigma}}^0 + \varepsilon\hat{\boldsymbol{\sigma}}^1 = \mathbb{B}(\varepsilon^{-1}\hat{\mathbf{e}}^{-1} + \hat{\mathbf{e}}^0 + \varepsilon\hat{\mathbf{e}}^1) + o(\varepsilon) \tag{3}$$

Equation (3) is true $\forall\varepsilon$, thus the following conditions are derived:

$$\mathbf{0} = \mathbb{B}(\hat{\mathbf{e}}^{-1}) \tag{4a}$$

$$\hat{\boldsymbol{\sigma}}^0 = \mathbb{B}(\hat{\mathbf{e}}^0) \tag{4b}$$

By considering Eq. (A.8) and the positive definiteness of the tensor $\mathbb{B}$, Eq. (4a) gives:

$$\hat{\mathbf{u}}^0_{,3} = 0 \Rightarrow [\hat{\mathbf{u}}^0] = \mathbf{0} \tag{5}$$

Moreover, substituting Eq. (A.9) written for $k = 0$ into Eq. (4b) it gives:

$$\hat{\boldsymbol{\sigma}}^0\mathbf{i}_j = \mathbf{K}^{1j}\hat{\mathbf{u}}^0_{,1} + \mathbf{K}^{2j}\hat{\mathbf{u}}^0_{,2} + \mathbf{K}^{3j}\hat{\mathbf{u}}^1_{,3} \tag{6}$$

with $j = 1, 2, 3$ and $\mathbf{K}^{jl}$ being the two-order tensors such that $K^{jl}_{ki} := B_{ijkl}$. Next, integrating Eq. (6) with respect to z_3 (for $j = 3$) and considering Eq. (A.17) it results:

$$[\hat{\mathbf{u}}^1] = (\mathbf{K}^{33})^{-1}\left(\hat{\boldsymbol{\sigma}}^0\mathbf{i}_3 - \mathbf{K}^{\alpha 3}\hat{\mathbf{u}}^0_{,\alpha}\right) \tag{7}$$

Then, by replacing Eq. (6) ($j = 1, 2$) in the equilibrium equation (A.18) one obtains:

$$(\hat{\boldsymbol{\sigma}}^1\mathbf{i}_3)_{,3} = -(\hat{\boldsymbol{\sigma}}^0\mathbf{i}_\alpha)_{,\alpha} = -(\mathbf{K}^{1\alpha}\hat{\mathbf{u}}^0_{,1} + \mathbf{K}^{2\alpha}\hat{\mathbf{u}}^0_{,2} + \mathbf{K}^{3\alpha}\hat{\mathbf{u}}^1_{,3})_{,\alpha} \tag{8}$$

Next, by integrating Eq. (8) with respect to z_3 between $-1/2$ and $1/2$ and by using Eq. (7), it is obtained:

$$\left[\hat{\boldsymbol{\sigma}}^1\mathbf{i}_3\right] = \Big(- \mathbf{K}^{\beta\alpha}\hat{\mathbf{u}}^0_{,\beta} - \mathbf{K}^{3\alpha}(\mathbf{K}^{33})^{-1}\left(\hat{\boldsymbol{\sigma}}^0\mathbf{i}_3 - \mathbf{K}^{\beta 3}\hat{\mathbf{u}}^0_{,\beta}\right) \Big)_{,\alpha} \tag{9}$$

where Greek indexes ($\alpha, \beta = 1, 2$) are related to the in-plane (x_1, x_2) quantities. Note that in Eq. (9) higher order effects, related to in-plane derivatives, appear. These terms, usually neglected in standard zero-order theories [23, 25], are related to the curvature of the deformed interface (second-order derivatives).

Finally, the transition from the rescaled configuration to the limit configuration is obtained by introducing the matching conditions Eqs.(A.27)-(A.30) and the interface laws at both zero-order and one-order are derived:

- Zero-order interface law:

$$[[\mathbf{u}^0]] = \mathbf{0} \tag{10}$$

$$[[\boldsymbol{\sigma}^0\ \mathbf{i}_3]] = \mathbf{0} \tag{11}$$

- One-order interface law:

$$[[\mathbf{u}^1]] = (\mathbf{K}^{33})^{-1}\left(\boldsymbol{\sigma}^0\mathbf{i}_3 - \mathbf{K}^{\alpha 3}\mathbf{u}^0_{,\alpha}\right) - \langle\langle \mathbf{u}^0_{,3}\rangle\rangle \tag{12}$$

$$[[\boldsymbol{\sigma}^1\ \mathbf{i}_3]] = \Big(-\mathbf{K}^{\beta\alpha}\mathbf{u}^0_{,\beta} - \mathbf{K}^{3\alpha}(\mathbf{K}^{33})^{-1}\left(\boldsymbol{\sigma}^0\mathbf{i}_3 - \mathbf{K}^{\beta 3}\mathbf{u}^0_{,\beta}\right)\Big)_{,\alpha} - \langle\langle \boldsymbol{\sigma}^0_{,3}\mathbf{i}_3\rangle\rangle \tag{13}$$

Equations (10)-(11) are the standard perfect interface condition, characterized by the continuity in terms of displacements and stresses at the interface [4]. Equations (12)-(13) are the displacements and stresses jumps at the interface in the one-order asymptotic theory. They depend on the displacements and the stresses fields at the zero-order and on their first and second-order derivatives.

The hard interface law in the reference configuration (Fig.2a) is derived by considering asymptotic expansions (A.14a) and (A.5a) combined with Eqs. (10)-(13) [25]:

$$[[\mathbf{u}^\varepsilon]] \approx \ \varepsilon\Big((\mathbf{K}^{33})^{-1}\left(\langle\langle\boldsymbol{\sigma}^\varepsilon\mathbf{i}_3\rangle\rangle - \mathbf{K}^{\alpha 3}\langle\langle\mathbf{u}^\varepsilon_{,\alpha}\rangle\rangle\right) - \langle\langle\mathbf{u}^\varepsilon_{,3}\rangle\rangle\Big) \tag{14}$$

$$[[\boldsymbol{\sigma}^\varepsilon\ \mathbf{i}_3]] \approx \varepsilon\Big(\Big(- \mathbf{K}^{\beta\alpha}\langle\langle\mathbf{u}^\varepsilon_{,\beta}\rangle\rangle - \mathbf{K}^{3\alpha}(\mathbf{K}^{33})^{-1}\left(\langle\langle\boldsymbol{\sigma}^\varepsilon\mathbf{i}_3\rangle\rangle - \mathbf{K}^{\beta 3}\langle\langle\mathbf{u}^\varepsilon_{,\beta}\rangle\rangle\right)\Big)_{,\alpha} - \langle\langle\boldsymbol{\sigma}^\varepsilon_{,3}\ \mathbf{i}_3\rangle\rangle\Big) \tag{15}$$

3. Introduction of the micro-cracking damage

In this section, it is shown how to include micro cracking damage in the hard interface law above obtained. The closed-form of the effective elastic tensors $\mathbf{K}^{jl}$ in Eqs. (14)-(15) is specialized by using micromechanical homogenization in the case of two microcracked material models: Kachanov-Sevostianov (KS) and Welemane-Goidescu (WG) models. The evolution law of the generalized microcracks density is derived from a thermodynamic approach and then included in the hard interface model via the asymptotic expansions method.

3.1. Micromechanical homogenization approaches

The Kachanov-Sevostianov model [32, 37] is a stress-based approach based on the non-interacting microcracks approximation [35, 36]. The Welemane-Goidescu model [40, 49, 50] is a strain-based approach, based on the dilute limit hypothesis [39]. For both models, it is assumed that the material interphase comprises an orthotropic matrix embedding a family of microcracks parallel to $\mathbf{i}_1$. For the sake of simplicity, the formulations are reduced to the two-dimensional case on the plane ($\mathbf{i}_1$, $\mathbf{i}_3$) with reference to the problem geometry in Fig.2.

3.1.1. Kachanov-Sevostianov model

Following the theory proposed by Kachanov and coworkers [32, 33] based on the Eshelby's approach [51], and the above assumptions on microcracks and matrix, the interface stiffness can be derived as follows:

$$
\begin{aligned}
K_{11}^{11} &= \frac{(E_1^0)^2\ (2\,R\,B_{nn}\,E_3^0\ +1)}{E_1^0 - E_3^0\,(\nu_{13}^0)^2 + 2\,R\,B_{nn}\,E_1^0\,E_3^0} \\
K_{31}^{13} = K_{13}^{31} &= \frac{E_1^0\,E_3^0\,\nu_{13}^0}{E_1^0 - E_3^0\,(\nu_{13}^0)^2 + 2\,R\,B_{nn}\,E_1^0\,E_3^0} \\
K_{33}^{33} &= \frac{E_1^0\,E_3^0}{E_1^0 - E_3^0\,(\nu_{13}^0)^2 + 2\,R\,B_{nn}\,E_1^0\,E_3^0} \\
K_{11}^{33} &= \frac{2\,G_{13}^0}{2 + R\,B_{tt}\,G_{13}^0}
\end{aligned}
\tag{16}
$$

where E_1^0, E_3^0, G_{13}^0, ν_{13}^0 and ν_{31}^0 are the in-plane elastic orthotropic moduli of the matrix; B_{nn} and B_{tt} are elastic parameters depending on the matrix and microcracks characteristics [32, 33].

Note that the engineering moduli can be also easily derived. The effective Young's modulus in normal direction ($\mathbf{i}_3$), used in the examples below, reads as:

$$
E_3 = \frac{E_3^0}{1 + 2\,R\,B_{nn}\,E_3^0} \tag{17}
$$

3.1.2. Welemane-Goidescu model

In [40, 49, 50, 52], Welemane and coworkers extended the energy-based homogenization approach originally proposed in [39] for isotropic materials to the case of an orthotropic matrix.

By following the Welemane-Goidescu model [49], the expressions of the interface stiffness read as:

$$
\begin{aligned}
K_{11}^{11} &= \frac{E_1^0}{E_3^0(\nu_{13}^0\nu_{31}^0-1)^2}\left(E_3^0(1-\nu_{13}^0\nu_{31}^0) - R\sqrt{E_3^0}(\nu_{31}^0)^2\pi\,\chi\right)\\
K_{31}^{13} = K_{13}^{31} &= \frac{E_1^0\nu_{31}^0}{(\nu_{13}^0\nu_{31}^0-1)^2}\left((1-\nu_{13}^0\nu_{31}^0) - R\sqrt{E_3^0}\pi\,\chi\right)\\
K_{33}^{33} &= \frac{E_3^0}{(\nu_{13}^0\nu_{31}^0-1)^2}\left((1-\nu_{13}^0\nu_{31}^0) - R\sqrt{E_3^0}\pi\,\chi\right)\\
K_{11}^{33} &= G_{13}^0\left(1 - R\frac{\pi}{\sqrt{E_1^0}}G_{13}^0\,\chi\right)
\end{aligned}
\tag{18}
$$

where $\chi = \left(\frac{1}{G_{13}^0} - 2\frac{\nu_{13}^0}{E_1^0} + \frac{2}{\sqrt{E_1^0E_3^0}}\right)^{\frac{1}{2}}$, and E_1^0, E_3^0, G_{13}^0, ν_{13}^0 and ν_{31}^0 are the in-plane elastic orthotropic moduli of the matrix.

Also in this case, the engineering moduli can be derived. The effective Young's modulus in normal direction ($\mathbf{i}_3$), adopted for next examples below, reads as:

$$
E_3 = E_3^0\,(1 - 2\,R\,H_{nn}\,E_3^0) \tag{19}
$$

with H_{nn} an elastic parameter depending on the matrix and microcracks characteristics [49] (analogous to the parameter B_{nn} of the KS model).

3.2. Damage evolution law

The proposed hard interface law expressed by Eqs. (12)-(13) in the limit configuration (Fig. 2c), or by Eqs. (14)-(15) in the reference configuration (Fig. 2a), depends on the generalized microcracks density R via the effective stiffness tensors expressed by Eqs. (16) and Eqs. (18) for the KS and WG model, respectively.

A possible evolution law of R in the interphase $\mathcal{B}^\varepsilon$ (of thickness ε) is herein derived following a thermodynamic approach [6, 7]. A pseudo-potential of dissipation Φ given by the sum of a quadratic term and a positively 1-homogeneous functional is considered [7]. The dissipative character of the evolution of damage is given by the rate-dependent form of the potential:

$$\Phi(\dot{R}) = \frac{1}{2}\,\eta^{\varepsilon}\dot{R}^2 + I_{[0,+\infty[}(\dot{R}), \tag{20}$$

where η^{ε} is a positive viscosity parameter; $I_{\mathcal{A}}$ denotes the indicator function of the set $\mathcal{A}$, i.e. $I_{\mathcal{A}}(x) = 0$ if $x \in \mathcal{A}$ and $I_{\mathcal{A}}(x) = +\infty$ otherwise; $\dot{R}$ is the increment of microcracks density compared to its initial level, indicated in what follows as R_0. The term $I_{[0,+\infty[}(\dot{R})$ forces $\dot{R}$ to assume non-negative values and it gives the irreversible character of the degradation process for a non-regenerative microcracked material ($R \geq R_0$).

The free energy associated with the constitutive equation of the microcracked material is chosen as follows:

$$\Psi\left(\mathbf{e}(\mathbf{u}^{\varepsilon}), R\right) = \frac{1}{2}\,\mathbb{B}^{\varepsilon}(R)\left(\mathbf{e}(\mathbf{u}^{\varepsilon}) : \mathbf{e}(\mathbf{u}^{\varepsilon})\right) - \omega^{\varepsilon} R + I_{[R_0,+\infty[}(R) \tag{21}$$

where $\mathbb{B}^{\varepsilon}(R)$ is the effective stiffness tensor of the material (obtained via the KS or WG model); $\mathbf{u}$ is the displacement field; $\mathbf{e}(\mathbf{u})$ is the strain tensor under the small perturbation hypothesis; ω^{ε} is a strictly negative parameter. Note that the irreversible character of damage, already imposed in Eq. (20), allows to neglect the term $I_{[R_0,+\infty[}(R)$ in Eq. (21).

By deriving Eqs. (20) and (21) with respect $\dot{R}$ and R respectively, then by replacing them into the movement equations in $\mathcal{B}^{\varepsilon}$ (for further details refer to [6, 53]), the following damage evolution law for $\dot{R}$ in the volume $\mathcal{B}^{\varepsilon}$ is obtained:

$$\eta^{\varepsilon}\dot{R} = \left(\omega^{\varepsilon} - \frac{1}{2}\,\mathbb{B}^{\varepsilon}_{,R}(R)\left(\mathbf{e}(\mathbf{u}^{\varepsilon}) : \mathbf{e}(\mathbf{u}^{\varepsilon})\right)\right)_{+} \tag{22}$$

where $(\cdot)_+$ denotes the positive part of the function and $\mathbb{B}^{\varepsilon}_{,R}(R)$ indicates the component-wise derivative of the stiffness tensor with respect to the generalized microcracks density R.

3.2.1. Asymptotic theory

In this section, the asymptotic behavior of the volumetric damage evolution law (Eq. (22)) is studied. It is prescribed that η^{ε} and ω^{ε} are volumetric densities and thus they are inversely proportional to the non-dimensional interphase thickness ε: $\eta^{\varepsilon} = \eta\,\varepsilon^{-1}$ and $\omega^{\varepsilon} = \omega\,\varepsilon^{-1}$, with $\eta > 0$ and $\omega < 0$. Subsequently, for the sake of simplicity, we will further assume that ω and η do not depend on the direction orthogonal to the interface surface x_3 (respectively z_3, in the rescaled configuration). In the following, also R is supposed to be independent of x_3 (respectively z_3).

Let focus on the term: $\dfrac{1}{2}\,\mathbb{B}^{\varepsilon}_{,R}(R)\,(\mathbf{e}(\mathbf{u}^{\varepsilon}) : \mathbf{e}(\mathbf{u}^{\varepsilon}))$ in Eq. (22). This term can be developed at 0-order as $\dfrac{1}{2}\,\mathbb{B}^{\varepsilon}_{,R}(R)\left(\hat{\mathbf{e}}^0 : \hat{\mathbf{e}}^0\right)$ and the constitutive equation (4b) leads to $\dfrac{1}{2}\,\mathbb{B}^{\varepsilon}_{,R}(R)\left[(\mathbb{B}^{\varepsilon})^{-1}(R)\,\hat{\sigma}^0 : \hat{\mathbf{e}}^0\right]$. Note that:

$$\hat{\mathbf{e}}^0 = Sym(\hat{u}^0_{,1} \otimes i_1 + \hat{u}^0_{,2} \otimes i_2 + \hat{u}^1_{,3} \otimes i_3) \tag{23}$$

where Sym gives the symmetric part of the enclosed tensor. This term is integrated along z_3 and gives $\dfrac{1}{2}\,\mathbb{B}^{\varepsilon}_{,R}(R)\left[(\mathbb{B}^{\varepsilon})^{-1}(R)\,\hat{\sigma}^0 : \langle\hat{\mathbf{e}}^0\rangle\right]$ or $\dfrac{1}{2}\,\mathbb{B}^{\varepsilon}_{,R}(R)\left(\hat{\mathbf{e}}^0 : \langle\hat{\mathbf{e}}^0\rangle\right)$. Next, by integrating again along z_3, it gives $\dfrac{1}{2}\,\mathbb{B}^{\varepsilon}_{,R}(R)\left(\langle\hat{\mathbf{e}}^0\rangle : \langle\hat{\mathbf{e}}^0\rangle\right)$, where

$$\langle\hat{\mathbf{e}}^0\rangle = Sym(\hat{u}^0_{,1} \otimes i_1 + \hat{u}^0_{,2} \otimes i_2 + [\hat{u}^1] \otimes i_3) \tag{24}$$

Finally, by adopting the following approximation:

$$Sym(\hat{u}^0_{,1} \otimes i_1 + \hat{u}^0_{,2} \otimes i_2 + [\hat{u}^1] \otimes i_3) \approx\ Sym(\hat{u}^{\varepsilon}_{,1} \otimes i_1 + \hat{u}^{\varepsilon}_{,2} \otimes i_2 + \frac{1}{\varepsilon}[\hat{u}^{\varepsilon}] \otimes i_3) \tag{25}$$

the (internal) damage evolution equation reads:

$$\eta \dot{R} = \left\{ \omega - \frac{1}{2}\, K^{\varepsilon}_{,R}(R) \begin{pmatrix} \langle u^{\varepsilon}_{,1} \rangle \\ \langle \hat{u}^{\varepsilon}_{,2} \rangle \\ [\hat{u}^{\varepsilon}] \end{pmatrix} \cdot \begin{pmatrix} \langle \hat{u}^{\varepsilon}_{,1} \rangle \\ \langle \hat{u}^{\varepsilon}_{,2} \rangle \\ [\hat{u}^{\varepsilon}] \end{pmatrix} \right\}_{+} \tag{26}$$

where

$$K^{\varepsilon} = \begin{pmatrix} \varepsilon K^{11} & \varepsilon K^{12} & K^{13} \\ \varepsilon K^{12} & \varepsilon K^{22} & K^{23} \\ K^{13} & K^{23} & \frac{1}{\varepsilon} K^{33} \end{pmatrix}$$

By introducing the matching conditions of the hard interface law (Eqs. (14)-(15)) and neglecting the second-order terms, the final form of the proposed damage evolution law for a hard interface model reads:

$$\eta \dot{R} = \left\{ \omega - \frac{1}{2}\, K_{,R}(R) \begin{pmatrix} \langle\langle u^{\varepsilon}_{,1} \rangle\rangle \\ \langle\langle u^{\varepsilon}_{,2} \rangle\rangle \\ [[u^{\varepsilon}]] + \varepsilon \langle\langle u^{\varepsilon}_{,3} \rangle\rangle \end{pmatrix} \cdot \begin{pmatrix} \langle\langle u^{\varepsilon}_{,1} \rangle\rangle \\ \langle\langle u^{\varepsilon}_{,2} \rangle\rangle \\ [[u^{\varepsilon}]] + \varepsilon \langle\langle u^{\varepsilon}_{,3} \rangle\rangle \end{pmatrix} \right\}_{+} \tag{27}$$

3.3. Connection of the generalized cracks density with normalized damage parameters

In the classical continuum damage theory at least one normalized damage variable is adopted to describe non-localized damage [6, 53, 54]. The simplest relationship to describe material properties degradation is $E = E^0(1 - D)$, where E^0 is the Young's modulus of the undamaged material and D is the damage variable going from 0 in undamaged conditions to 1 in fully damaged conditions. This damage description is generally used in commercial software for finite element analysis (FEA). Connection relationships between D and the generalized cracks density R can be obtained for both KS and WG model by using Eq.(17) and Eq.(19), respectively, and they read as:

$$
\begin{aligned}
&D = \frac{2\,R\,B_{nn}\,E^0}{1 + 2\,R\,B_{nn}\,E^0} \qquad \textit{for KS model}\\
&D = 2\,R\,H_{nn}\,E^0 \qquad \textit{for WG model}
\end{aligned}
\tag{28}
$$

Equations (28) show that in undamaged conditions $D = R = 0$ for both damaged-material models. Instead, in fully damaged conditions ($D = 1$), $R \to +\infty$ for the KS model and it is bounded by the value $R = 1/2\,H_{nn}\,E^0$ for the WG model. Note that to have a upper bound for R, in the WG model, is consistent with the dilute limit theory, on which the WG model is based [40], meaning that the model is valid for small density values. These connection relationships (28) have a twofold advantage: (i) they allow a microstructural interpretation of the damage variable D, by making explicit its dependency on material and microcracks properties; (ii) they are expected to simplify the implementation of the proposed interface model in commercial FEA-software for future validation with numerical simulation.

4. Numerical examples

Hereafter, two academic examples are used to illustrate the constitutive and structural behavior of the proposed hard interface model with micro-cracking damage. All the numerical computations have been carried out using the commercial software *Mathematica* [55].

4.1. 0-D example: The constitutive behavior

In this section, a 0-D example is developed to illustrate the constitutive behavior of the interface model. Different points are discussed: the comparison between damaged material models KS and WG; the influence of damage parameters η and ω on the interface law; and finally, the influence of the loading rate and of cyclic loads on the interface behavior.

4.1.1. Effects of the damage evolution law

The mechanical properties of the damaged material (Young's modulus $E_d(E_u, R)$) in the case of KS (Eq. (17)) and WG (Eq. (19)) models, read as follows:

$$\begin{aligned} E_d^{KS}(E_u, R) &= \frac{E_u}{1+2\,\pi\,R} \qquad \textit{for KS model} \\ E_d^{WG}(E_u, R) &= E_u\,(1-2\,\pi\,R) \qquad \textit{for WG model} \end{aligned} \tag{29}$$

where $B_{nn} = H_{nn} = \frac{\pi}{E_u}$. By deriving with respect R one obtains:

$$\begin{aligned} (E_d^{KS})_{,R} &= -\frac{2\,\pi\,E_u}{(1+2\,\pi\,R)^2} \qquad \textit{for KS model} \\ (E_d^{WG})_{,R} &= -2\,\pi\,E_u \qquad \textit{for WG model} \end{aligned} \tag{30}$$

The damage evolution laws in the 0-D case, for both KS and WG models, are obtained substituting Eqs. (30) into Eq. (27):

$$\eta\dot{R} = \begin{cases} \left(\omega - \dfrac{1}{2}\dfrac{(E_d^{KS})_{,R}}{\varepsilon}\,[u]_n^2\right)_+ & \textit{for KS model} \\ \left(\omega - \dfrac{1}{2}\dfrac{(E_d^{WG})_{,R}}{\varepsilon}\,[u]_n^2\right)_+ & \textit{for WG model} \end{cases} \tag{31}$$

Equations (31) have been numerically solved with an imposed displacement jump equal to $[u]_n = [u]_{max}\,\frac{t}{t_f}$ with $[u]_{max} = 0.1$ mm and $t_f = 5$ s. Note that the time unit (s) is only qualitative and the proposed model does not depend on it because the interface model is developed in a quasi-static framework. Moreover, let $E_u = 70 \times 10^3$ MPa and $\varepsilon = 2$ mm. The chosen reference values for damage parameters are $\eta = 30$ MJ.s/mm^2 and $\omega = -2$ MJ/mm^2. Initial damage was imposed to vanish ($R_0 = 0$). To investigate the effects of parameters η and ω on the interface model, a one-factor-a-time (OFAT) study on both η and ω has been made on ranges $\eta = (0.3, 3, 30, 300)$ and $\omega = (-0.2, -2, -20, -200)$.

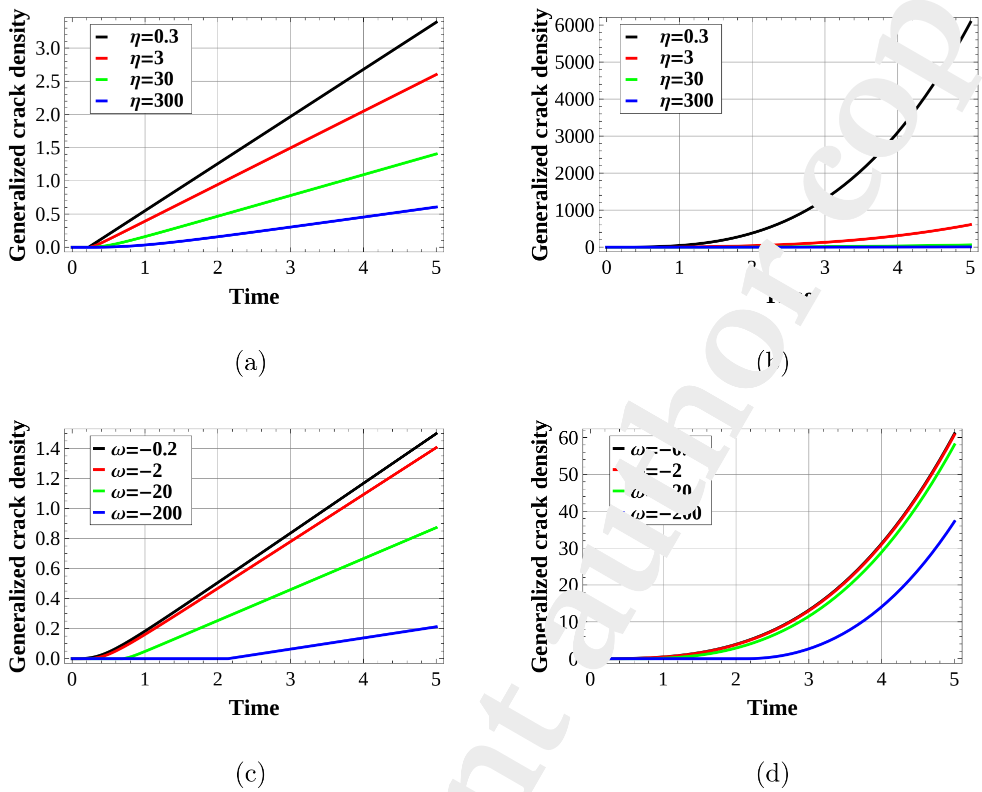

Fig. 3: Evolution of the generalized microcracks density R. Fig. 3(a): effect of varying η in the KS model. Fig. 3(b): effect of varying η in the WG model. Fig. 3(c): effect of varying ω in the KS model. Fig. 3(d): effect of varying ω in the WG model.

Figures 3a-d show the evolution of the generalized microcracks density R as a function of the time and of damage parameters η and ω, for both KS and WG models. At the beginning, both models present an horizontal plateau at zero (because of the imposed initial damage $R_0 = 0$); then, after damage initiation, a linear increasing behavior is found for the KS model and a cubic increasing behavior for the WG model. An inverse proportionality between R and η is found in both models (see Fig. 3(a) and Fig. 3(b)), this highlights that η has the physical meaning of a damage viscosity influencing the velocity (slope of (R, t) curves) of the damage evolution. This result is also emphasized in Fig. 4, where the degradation of the Young's modulus of both damaged materials KS and WG is shown. The slope of $(E_d/Eu, t)$ curves, for both KS and WG models, increases as η decreases, meaning that material get damaged "faster" for smaller values of η.

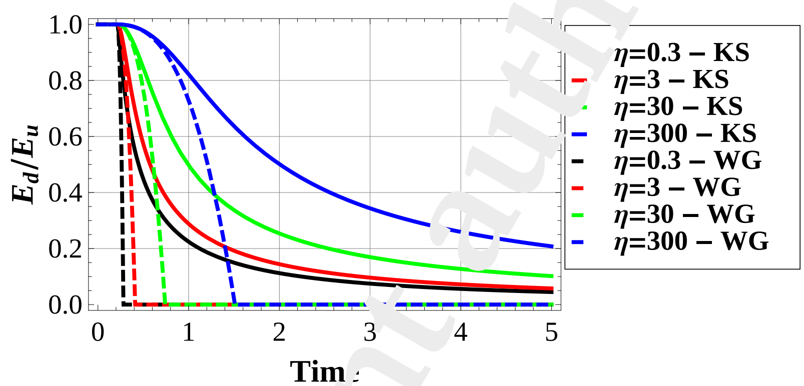

Fig. 4: Evolution in time of the Young's modulus of the damaged materials: parametric study on η. Kachanov-Sevostianov (KS, solid lines) and Welemane-Goidescu (WG, dashed lines) damaged material models are represented.

The parameter ω has the physical meaning of a threshold energy beyond which damage initiates, in analogy with Dupré's energy for adhesion [53]. In fact, the damage-initiation time, *i.e.*, when R begins to increase, is more influenced by ω than by η for both damaged materials, as highlighted in Figs. 3(c), 3(d) and 5.

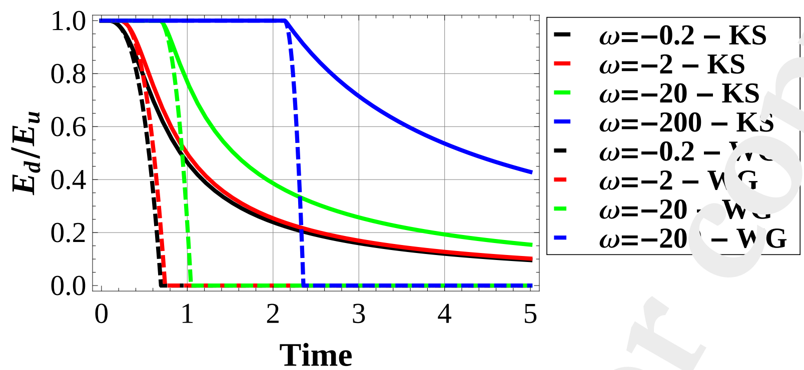

Fig. 5: Evolution in time of the Young's modulus of the damaged materials: parametric study on ω. Kachanov-Sevostianov model (KS, solid lines) and Welemane-Goidescu model (WG, dashed lines).

Moreover, Figs. 4 and 5 show that the complete damage (*i.e.*, when E_d tends to zero) occurs earlier for the WG model than for the KS model independently of ω and η. Note that in the case of KS model, E_d tends to zero asymptotically (data not shown). This different behavior of the two models is consistent with the two different hypotheses on which the models are based. Particularly, WG model is based on the dilute limit hypothesis, meaning that it is valid for small density values (less than 20% according to [39]). This is also in agreement with the fact that the generalized cracks density R has an upper bound in the case of WG model (see Section 3.3). The KS model is based on the non interacting microcracks approximation and it is valid for greater microcracks densities (until 80% according to [36, 37]). For further details regarding the difference between these microstructural hypotheses the reader can refer to [37].

The interface model in 0-D can be expressed as:

$$\sigma_n = \frac{E_d}{\varepsilon}\,[u]_n \tag{32}$$

Equation (32) has been solved for both KS and WG models, replacing E_d by E_d^{KS} and E_d^{WG}, respectively (see Eqs. (29)), in which R has been obtained by Eqs. (31).

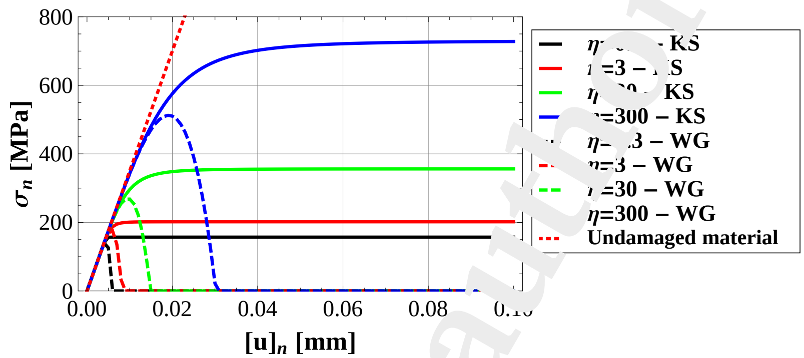

Fig. 6: Interface law: parametric study on η. Kachanov-Sevostianov (KS, solid lines) and Welemane-Goidescu (WG, dashed lines) damaged material models are represented. The linear-elastic behavior of the undamaged material is represented with a red dotted line.

Figures 6 and 7 show the interface model for both damaged materials as a function of η and ω. Numerical curves are obtained by solving the damaged interface model (Eqs. (32), (29), and (31)) in displacement-controlled mode. Both figures suggest a brittle damage behavior in the case of WG model and a ductile damage behavior for the KS model. Figure 6 highlights that the

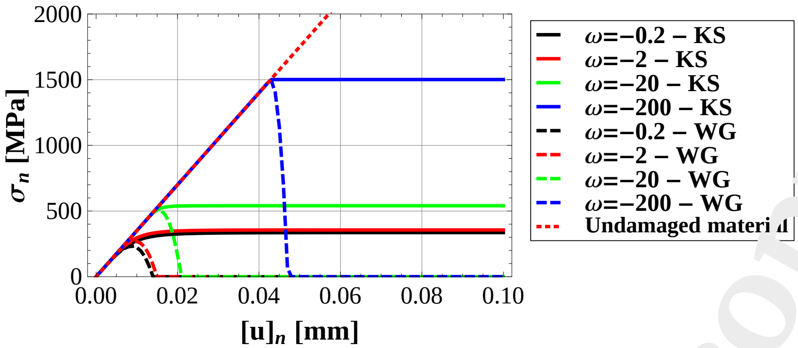

Fig. 7: Interface law: parametric study on ω. Kachanov-Sevostianov (KS, solid lines) and Welemane-Goidescu (WG, dashed lines) damage material models are represented. The linear-elastic behavior of the undamaged material is represented with a red dotted line.

elastic limit increases with η and this result confirms the role of the damage viscosity η as the velocity of the damage evolution. Figure 6 shows also that η influences the nonlinear transition between the linear elastic domain and the damaged domain (this is more evident in KS model than in WG model); thus for a small damage viscosity η this transition tends to vanish (*i.e.*, suggesting that the material gets damaged immediately after the initiation). Figure 7 emphasizes the role of parameter ω as a damage initiation threshold: thus the higher is ω, the later damage initiates (see Fig. 5) and the higher the elastic limit.

4.1.2. Effects of the loading rate

The influence of the loading rate and of the loading shape on the interface model has been investigated. In particular, two displacement jumps have been separately imposed to solve Eqs. (32), (29), and (31): a ramp function $[u]_n = v\,t$ and a quadratic function $[u]_n = 1/2\,v^2\,t^2 + 1/2\,v\,t$. Four values of the loading rate $v = [u]_{max}/t_f$ have been simulated $(0.1, 0.2, 2, 20)$ mm/s with a fixed $[u]_{max} = 1\,\text{mm}$ and by varying the duration t_f between $(0.05, 0.5, 5, 10)$ s. The damage parameters have been taken equal to their reference values $\eta = 30$ MJ.s/mm^2 and $\omega = -2$ MJ/mm^2. The other parameters $E_u = 70 \times 10^3$ MPa, $\varepsilon = 2$ mm and $R_0 = 0$, are taken as in the previous study.

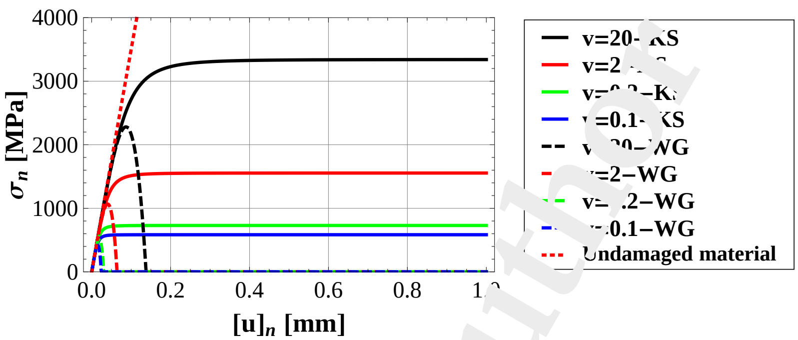

Fig. 8: Interface law for a ramp displacement jump: parametric study on the loading rate v. Kachanov-Sevostianov (KS, solid lines) and Welemane-Goidescu (WG, dashed lines) damaged material models are represented. The linear-elastic behavior of the undamaged material is represented with a red dotted line.

Figure 8 shows the interface law in the case of the ramp displacement jump. In analogy with the previous section, a ductile damage behavior of the interface is obtained in the case of KS model and a brittle damage behavior for WG model.

Figure 9 shows the interface law in the case of the quadratic displacement jump. The imposed quadratic displacement jump produces an hardening-like

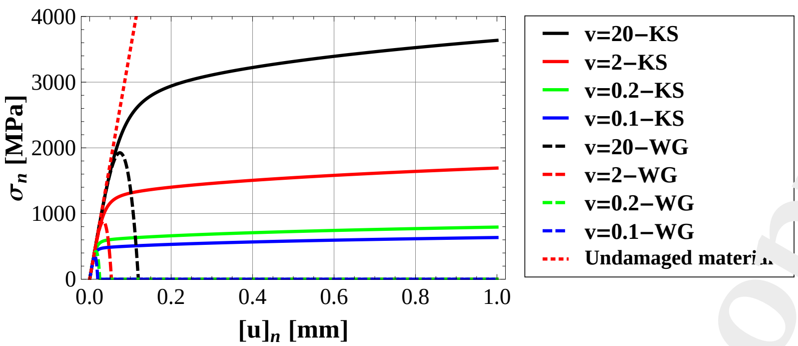

Fig. 9: Interface law for a quadratic displacement-jump: parametric study on the loading rate v. Kachanov-Sevostianov (KS, solid lines) and Welemane-Goidescu (WG, dashed lines) damaged material models are represented. The linear-elastic behavior of the undamaged material is represented with a red dotted line.

effect in the damaged part of the interface constitutive behavior (*i.e.*, beyond the elastic limit) and the slope increases with the loading rate v.

Both Figs. 8-9 highlight that for high rates ($v = 2$, 20 mm/s) the elastic limit (tensile) is higher than in the quasi-static configurations ($v = 0.1$, 0.2 mm/s) for both KS and WG models. Recently, authors provide a validation of the proposed hard interface model in [31], by comparing simulated response curves with data from tensile experimental tests available in the literature [56] in both quasi-static and high-rate loading conditions. They found that the loading-rate dependence of the hard interface model makes it suitable to describe the experimental behavior observed in [56].

4.1.3. Effects of cyclic loading

The influence of cyclic loading on the hard interface model has also been investigated. A strictly positive sinusoidal displacement jump has been imposed: $[u]_n = [u]_{max} |\sin(f\,t/t_f)|$, with $[u]_{max} = 1\,\text{mm}$, $f = \pi/2$, $t_f = 5$ s and 5 cycles have been considered. Both KS and WG damage models have been considered and the damage parameters have been taken equal to their reference values $\eta = 30$ MJ.s/mm^2 and $\omega = -2$ MJ/mm^2. $E_u = 70 \times 10^3$ MPa, $\varepsilon = 2$ mm and $R_0 = 0$, as in the previous study.

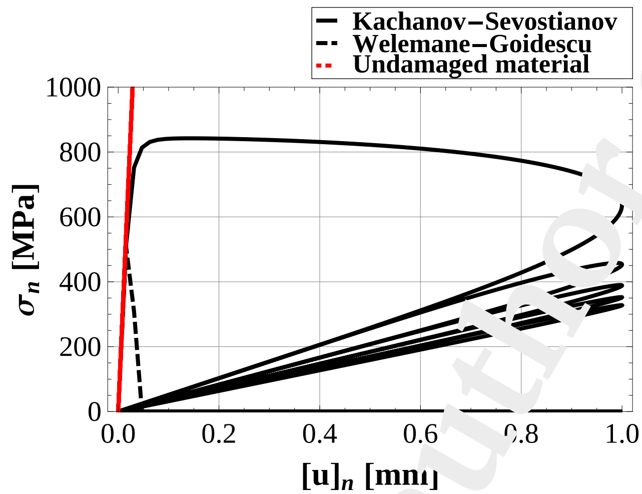

Fig. 10: Interface law for a cyclic load for KS and WG model. The linear-elastic behavior of the undamaged material is represented with a red dotted line.

As shown in Fig. 10, the two damage models give very different results under the same loading and parameter conditions. KS model, together with the proposed damage evolution law, is able to reproduce an elastic-damaged material behavior with hysteresis, as illustrated in Fig. 10. Generally, the energy dissipated via micro-cracking damage is higher at the initiation and first accumulation of microcracks. This is consistent with the resulting hysteresis loop of the first cycle that is larger than the others; after the first cycle, the hysteresis decreases with the number of cycles until the damage evolution is completed. Moreover, the damage evolution produces a decreasing of the interface stiffness (see Fig. 10). The stiffness of the undamaged material is equal to 35000 N/mm^3 and after the first cycle it reduces to 515 N/mm^3. After the first reloading (2nd cycle), the stiffness slightly decreases until the damage evolution is completed, and at the end of the fifth cycle the stiffness is equal to 318 N/mm^3. This result is physically plausible.

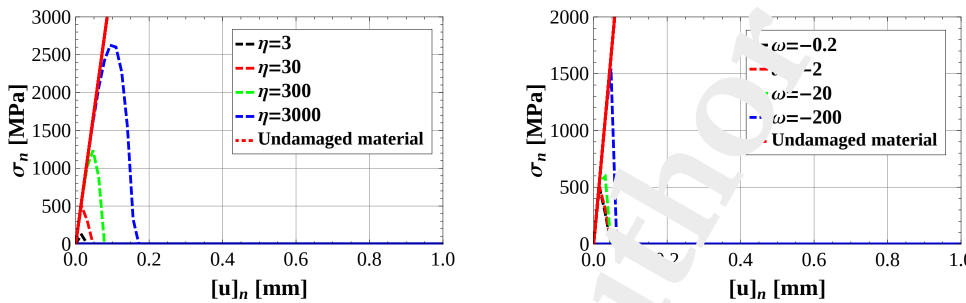

(a) (b)

Fig. 11: Interface law for a cyclic load for WG model. Fig. 11(a): study on η. Fig. 11(b): study on ω.

On the contrary, WG damage model is not able to reproduce a damage behavior under cyclic loads. Figure 10 shows an abrupt reduction in stiffness to zero already during the first loading curve, meaning that the damaged material behavior is brittle, in agreement with the previous results. Note that this behavior does not depend on the chosen values of the damaged parameters η and ω as illustrated in Fig. 11.

Finally, Fig. 12 shows the evolution in time of the normal stress σ_n in the case of KS model, highlighting the decrease of the maximum normal stress with the number of cycles (note a decrease of the 60% at the last cycle).

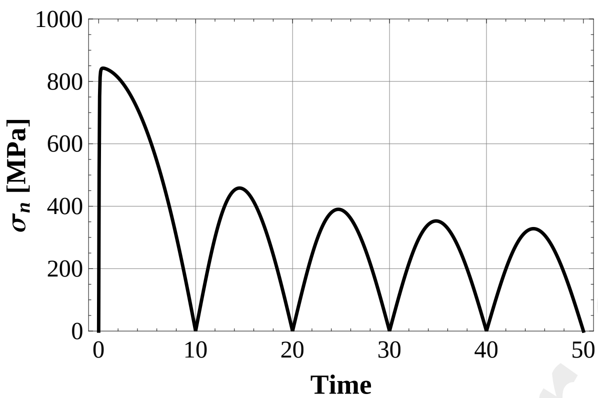

Fig. 12: Interface law for a cyclic load: normal stress as a function of the time for the Kachanov-Sevostianov damage model.

4.2. 1-D example: The structural behavior

In this section, a simple 1-D example is developed to illustrate the structural behavior of the proposed hard interface model. A composite bar under traction was considered. The bar, of section A, comprised two parts of length ℓ, made of an undamaged material with Young's modulus E_u, and an embedded part of length ε, made of a damageable material (glue-like interphase) with Young's modulus $E_d(E_u, R)$. The damageable material in the interphase is supposed to have at the beginning the same Young's modulus of the adherents, then it degrades as the microcracks density R evolves. The bar was fixed at one end and a quasi-static traction force was $F(t)$ applied on the other end, as illustrated in Fig. 13.

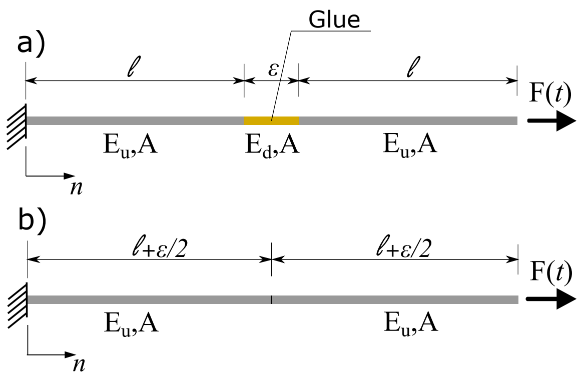

Fig. 13: 1-D example: bar under traction, a) glue interphase, b) interface model

The displacement field can be easily derived analytically as:

$$u(n) = \begin{cases} \dfrac{F}{E_u\,A} n & 0 \le n \le \ell \\ \dfrac{F}{E_d\,A} n + \dfrac{F\,\ell}{A}\left(\dfrac{1}{E_u} - \dfrac{1}{E_d}\right) & \ell \le n \le \ell + \varepsilon \\ \dfrac{F}{E_u\,A} n - \dfrac{F\,\varepsilon}{A}\left(\dfrac{1}{E_u} - \dfrac{1}{E_d}\right) & \ell + \varepsilon \le n \le 2\ell + \varepsilon \end{cases} \tag{33}$$

Thus, the displacement jump along n is obtained as $[u]_n = u(\ell + \varepsilon) - u(\ell)$:

$$[u]_n = \frac{F\,\varepsilon}{E_d\,A} \tag{34}$$

Note that, being $\frac{F}{A} = \sigma_n$, the standard spring-like interface law in 1-D approximation can be derived (in analogy with Eq. (32)).

The Young's modulus of the damaged material $E_d(E_u, R)$ was specialized to the case of KS and WG model following Eqs. (29) as in the previous example. The expression of the evolution of damage Eqs. (31) taking into account the displacement jump Eq. (34) is derived in this 1-D case as:

$$\dot{R} = \begin{cases} \dfrac{1}{\eta}\left(\omega + \pi \dfrac{\sigma_n^2}{E_u}\,\varepsilon\right)_+ & \textit{for KS model} \\ \dfrac{1}{\eta}\left(\omega + \pi \dfrac{\sigma_n^2}{E_u}\,\varepsilon\,\dfrac{1}{(1 - 2\pi\,R)^2}\right)_+ & \textit{for WG model} \end{cases} \tag{35}$$

where $\sigma_n = \bar{\sigma}\,\bar{t}$ with $\bar{t} = \frac{t}{t_f} \in [0,\,1]$, $t_f = 5$ s and $\bar{\sigma} = 400$ MPa. Moreover, reference values are taken as previously: $E_u = 70 \times 10^3$ MPa, $\varepsilon = 2$ mm, $\eta = 30$ MJ.s/mm^2 and $\omega = -2$ MJ/mm^2.

The structural response of the proposed hard interface model, in terms of tensile stress as a function of the macroscopic displacement jump is illustrated in Fig. 14, where we find again a brittle behavior for WG material and a ductile behavior for KS material.

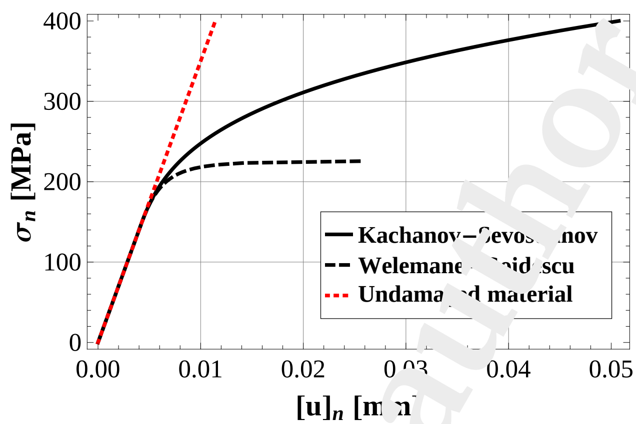

Fig. 14: Interface law in the 1-D case: Kachanov-Sevostianov model (KS, solid line), Welemane-Goidescu model (WG, dashed line), undamaged material (red dotted line).

5. Conclusions

This work proposes an original model of hard imperfect interface accounting for micro-cracking and damage evolution. Preliminary numerical results based on simple academic examples, in terms of both constitutive and structural behavior, are promising. They suggest that the model could represent a suitable strategy for a macroscopic description of hard adhesives with micro-cracking damage, regardless of whether they have a ductile or brittle behavior. In fact, the analytical interface model could be included in a finite element context via user-defined interface finite elements. Moreover, connection relationships between the generalized cracks density and the standard normalized damage variable, derived at Section 3.3, are expected to simplify the implementation in commercial FEA-software for future validation with numerical simulation.

The main perspective to enhance the proposed model is to establish a combined experimental/modelling identification protocol for the damage parameters of the evolution law, the damage viscosity η and the damage threshold ω. A design of experience will be set up in order to catch the interactions between damage parameters η and ω that we could only glimpse through the OFAT approach. To this aim, authors have specialized the proposed hard interface model to the case of tubular-butt joints under combined tensile-torsion loads [31]. This is a standard experimental design used to characterize structural adhesives and it allows future validations of the proposed interface model with experimental tests.

A. Matched asymptotic expansions method

A.1. Rescaling phase

The rescaling phase of the asymptotic process represents a mathematical construct [46], not a physically-based configuration, and it is used in order to eliminate the dependency of the integration domains on the small parameter

ε. This construct can also be seen as a change of spatial variables in the interphase domain [45, 46] $\hat{\mathbf{p}} := (x_1, x_2, x_3) \to (z_1, z_2, z_3)$:

$$z_1 = x_1, \qquad z_2 = x_2, \qquad z_3 = \frac{x_3}{\varepsilon} \tag{A.1}$$

resulting

$$\frac{\partial}{\partial z_1} = \frac{\partial}{\partial x_1}, \qquad \frac{\partial}{\partial z_2} = \frac{\partial}{\partial x_2}, \qquad \frac{\partial}{\partial z_3} = \varepsilon \frac{\partial}{\partial x_3} \tag{A.2}$$

as well as in the adherents $\bar{\mathbf{p}} := (x_1, x_2, x_3) \to (z_1, z_2, z_3)$:

$$z_1 = x_1, \qquad z_2 = x_2, \qquad z_3 = x_3 \pm \frac{1}{2}(1 - \varepsilon) \tag{A.3}$$

where the plus (minus) sign applies whenever $x \in \Omega^\varepsilon{}_+$ ($x \in \Omega^\varepsilon{}_-$), with

$$\frac{\partial}{\partial z_1} = \frac{\partial}{\partial x_1}, \qquad \frac{\partial}{\partial z_2} = \frac{\partial}{\partial x_2}, \qquad \frac{\partial}{\partial z_3} = \frac{\partial}{\partial x_3} \tag{A.4}$$

After the change of variables (A.1) and (A.3), the interphase occupies the domain $\mathcal{B} = \{(z_1, z_2, z_3) \in \mathbb{R}^3 : (z_1, z_2) \in \mathcal{S}, |z_3| < \frac{1}{2}\}$ and the adherents occupy the domains $\Omega_\pm = \Omega^\varepsilon{}_\pm \pm \frac{1}{2}(1 - \varepsilon)\mathbf{i}_3$, as shown in Fig. 2b. The sets $\mathcal{S}_\pm = \{(z_1, z_2, z_3) \in \mathbb{R}^3 : (z_1, z_2) \in \mathcal{S}, z_3 = \pm\frac{1}{2}\}$ are taken to denote the interfaces between $\mathcal{B}$ and $\Omega_\pm$ and $\Omega = \Omega_+ \cup \Omega_- \cup \mathcal{B} \cup \mathcal{S}_+ \cup \mathcal{S}_-$ is the rescaled configuration of the composite body. Γ_u and Γ_g indicate the images of Γ_u^ε and Γ_g^ε after the change of variables, and $\bar{\mathbf{f}}^\pm := \mathbf{f}^\pm \circ \bar{\mathbf{p}}^{-1}$ and $\bar{\mathbf{g}}^\pm := \mathbf{g}^\pm \circ \bar{\mathbf{p}}^{-1}$ the rescaled external forces.

A.2. Kinematic equations

Following the approach proposed in [23, 25], let us focus on the kinematics of the elastic problem. After taking $\hat{\mathbf{u}}^\varepsilon = \mathbf{u}^\varepsilon \circ \hat{\mathbf{p}}^{-1}$ and $\bar{\mathbf{u}}^\varepsilon = \mathbf{u}^\varepsilon \circ \bar{\mathbf{p}}^{-1}$ to denote the displacement fields from the rescaled adhesive and adherents, respectively, the asymptotic expansions of the displacement fields with respect to ε are:

$$\mathbf{u}^{\varepsilon}(x_1, x_2, x_3) = \mathbf{u}^0 + \varepsilon \mathbf{u}^1 + \varepsilon^2 \mathbf{u}^2 + o(\varepsilon^2) \tag{A.5a}$$

$$\hat{\mathbf{u}}^{\varepsilon}(z_1, z_2, z_3) = \hat{\mathbf{u}}^0 + \varepsilon \hat{\mathbf{u}}^1 + \varepsilon^2 \hat{\mathbf{u}}^2 + o(\varepsilon^2) \tag{A.5b}$$

$$\bar{\mathbf{u}}^{\varepsilon}(z_1, z_2, z_3) = \bar{\mathbf{u}}^0 + \varepsilon \bar{\mathbf{u}}^1 + \varepsilon^2 \bar{\mathbf{u}}^2 + o(\varepsilon^2) \tag{A.5c}$$

Interphase. The gradient of the displacement field $\hat{\mathbf{u}}^{\varepsilon}$ reads:

$$\nabla\left(\hat{\mathbf{u}}^{\varepsilon}\right) = \varepsilon^{-1} \begin{bmatrix} 0 & \hat{u}^0_{\alpha,3} \\ 0 & \hat{u}^0_{3,3} \end{bmatrix} + \begin{bmatrix} \hat{u}^0_{\alpha,\beta} & \hat{u}^1_{\alpha,3} \\ \hat{u}^0_{3,\beta} & \hat{u}^1_{3,3} \end{bmatrix} + \varepsilon \begin{bmatrix} \hat{u}^1_{\alpha,\beta} & \hat{u}^2_{\alpha,3} \\ \hat{u}^1_{3,\beta} & \hat{u}^2_{3,3} \end{bmatrix} + O(\varepsilon^2) \tag{A.6}$$

where $\alpha, \beta = 1, 2$, so that the strain tensor is:

$$\mathbf{e}(\hat{\mathbf{u}}^{\varepsilon}) = \frac{1}{2}\left[\nabla\left(\hat{\mathbf{u}}^{\varepsilon}\right) + \nabla\left(\hat{\mathbf{u}}^{\varepsilon}\right)^T\right] = \varepsilon^{-1}\hat{\mathbf{e}}^{-1} + \hat{\mathbf{e}}^0 + \varepsilon \hat{\mathbf{e}}^1 + O(\varepsilon^2) \tag{A.7}$$

with:

$$\hat{\mathbf{e}}^{-1} = \begin{bmatrix} 0 & \frac{1}{2}\hat{u}^0_{\alpha,3} \\ \frac{1}{2}\hat{u}^0_{\alpha,3} & \hat{u}^0_{3,3} \end{bmatrix} = Sym(\hat{\mathbf{u}}^0_{,3} \otimes \mathbf{i}_3) \tag{A.8}$$

$$\hat{\mathbf{e}}^k = \begin{bmatrix} Sym(\hat{u}^k_{\alpha,\beta}) & \frac{1}{2}(\hat{u}^k_{3,\alpha} + \hat{u}^{k+1}_{\alpha,3}) \\ \frac{1}{2}(\hat{u}^k_{3,\alpha} + \hat{u}^{k+1}_{\alpha,3}) & \hat{u}^{k+1}_{3,3} \end{bmatrix} = Sym(\hat{\mathbf{u}}^k_{,1} \otimes \mathbf{i}_1 + \hat{\mathbf{u}}^k_{,2} \otimes \mathbf{i}_2 + \hat{\mathbf{u}}^{k+1}_{,3} \otimes \mathbf{i}_3) \tag{A.9}$$

where $Sym(\cdot)$ gives the symmetric part of the enclosed tensor and $k = 0, 1$, and $\otimes$ is the dyadic product between vectors such as: $(\mathbf{a} \otimes \mathbf{b})_{ij} = a_i b_j$. Moreover, the following notation for derivatives is adopted: $f_{,j}$ denoting the partial derivative of f with respect to z_j.

Adherents. The gradient of the displacement field $\bar{\mathbf{u}}^{\varepsilon}$ reads:

$$\nabla\left(\bar{\mathbf{u}}^{\varepsilon}\right)=\begin{bmatrix}\bar{u}^0_{\alpha,\beta} & \bar{u}^0_{\alpha,3}\\ \bar{u}^0_{3,\beta} & \bar{u}^0_{3,3}\end{bmatrix}+\varepsilon\begin{bmatrix}\bar{u}^1_{\alpha,\beta} & \bar{u}^1_{\alpha,3}\\ \bar{u}^1_{3,\beta} & \bar{u}^1_{3,3}\end{bmatrix}+O(\varepsilon^2) \tag{A.10}$$

so that the strain tensor is:

$$\mathbf{e}(\bar{\mathbf{u}}^{\varepsilon})=\frac{1}{2}\left[\nabla\left(\bar{\mathbf{u}}^{\varepsilon}\right)+\nabla\left(\bar{\mathbf{u}}^{\varepsilon}\right)^T\right]=\varepsilon^{-1}\bar{\mathbf{e}}^{-1}+\bar{\mathbf{e}}^0+\varepsilon\bar{\mathbf{e}}^1+O(\varepsilon^2) \tag{A.11}$$

with:

$$\bar{\mathbf{e}}^{-1}=\mathbf{0} \tag{A.12}$$

$$\bar{\mathbf{e}}^k=\begin{bmatrix}Sym(\bar{u}^k_{\alpha,\beta}) & \frac{1}{2}(\bar{u}^k_{3,\alpha}+\bar{u}^k_{\alpha,3})\\ \frac{1}{2}(\bar{u}^k_{3,\alpha}+\bar{u}^k_{\alpha,3}) & \bar{u}^k_{3,3}\end{bmatrix}=Sym(\bar{\mathbf{u}}^k_{,1}\otimes\mathbf{i}_1+\bar{\mathbf{u}}^k_{,2}\otimes\mathbf{i}_2+\bar{\mathbf{u}}^k_{,3}\otimes\mathbf{i}_3) \tag{A.13}$$

and $k=0,1$.

A.3. Equilibrium equations

The stress fields in the rescaled adhesive and adherents, $\hat{\boldsymbol{\sigma}}^{\varepsilon}=\boldsymbol{\sigma}\circ\hat{\mathbf{p}}^{-1}$ and $\bar{\boldsymbol{\sigma}}^{\varepsilon}=\boldsymbol{\sigma}\circ\bar{\mathbf{p}}^{-1}$ respectively, can be represented as asymptotic expansions [23, 25]:

$$\boldsymbol{\sigma}^{\varepsilon}=\boldsymbol{\sigma}^0+\varepsilon\boldsymbol{\sigma}^1+O(\varepsilon^2) \tag{A.14a}$$

$$\hat{\boldsymbol{\sigma}}^{\varepsilon}=\hat{\boldsymbol{\sigma}}^0+\varepsilon\hat{\boldsymbol{\sigma}}^1+O(\varepsilon^2) \tag{A.14b}$$

$$\bar{\boldsymbol{\sigma}}^{\varepsilon}=\bar{\boldsymbol{\sigma}}^0+\varepsilon\bar{\boldsymbol{\sigma}}^1+O(\varepsilon^2) \tag{A.14c}$$

Interphase. As body forces are neglected, the equilibrium equation is:

$$div\hat{\boldsymbol{\sigma}}^{\varepsilon}=\mathbf{0} \tag{A.15}$$

Substituting Eq. (A.14b) in Eq. (A.15) and using Eq. (A.2), it becomes:

$$\begin{aligned} 0 &= \hat{\sigma}^{\varepsilon}_{i\alpha,\alpha} + \varepsilon^{-1}\hat{\sigma}^{\varepsilon}_{i3,3} \\ &= \varepsilon^{-1}\hat{\sigma}^{0}_{i3,3} + \hat{\sigma}^{0}_{i\alpha,\alpha} + \hat{\sigma}^{1}_{i3,3} + \varepsilon\hat{\sigma}^{1}_{i\alpha,\alpha} + O(\varepsilon) \end{aligned} \tag{A.16}$$

where $\alpha = 1, 2$. Eq. (A.16) has to be satisfied for any value of ε, leading to:

$$\hat{\sigma}^{0}_{i3,3} = 0 \tag{A.17}$$

$$\hat{\sigma}^{0}_{i1,1} + \hat{\sigma}^{0}_{i2,2} + \hat{\sigma}^{1}_{i3,3} = 0 \tag{A.18}$$

where $i = 1, 2, 3$.

Eq. (A.17) shows that $\hat{\sigma}^{0}_{i3}$ is not dependent on z_3 in the adhesive, and thus it can be written:

$$[\hat{\sigma}^{0}_{i3}] = 0 \tag{A.19}$$

where $[\cdot]$ denotes the jump between $z_3 = \frac{1}{2}$ and $z_3 = -\frac{1}{2}$. In view of Eq. (A.19), Eq. (A.18), for $i = 3$, can be rewritten in the integrated form

$$[\hat{\sigma}^{1}_{33}] = -\hat{\sigma}^{0}_{13,1} - \hat{\sigma}^{0}_{23,2} \tag{A.20}$$

Adherents. The equilibrium equation in the adherents is:

$$\mathrm{div}\bar{\boldsymbol{\sigma}}^{\varepsilon} + \bar{\mathbf{f}} = \mathbf{0} \tag{A.21}$$

Substituting Eq. (A.14c) in Eq. (A.21) that has to be satisfied for any value of ε, leads to:

$$\mathrm{div}\bar{\boldsymbol{\sigma}}^{0} + \bar{\mathbf{f}} = \mathbf{0} \tag{A.22}$$

$$\mathrm{div}\bar{\boldsymbol{\sigma}}^{1} = \mathbf{0} \tag{A.23}$$

A.4. Matching phase

The imposed continuity conditions at $\mathcal{S}^{\varepsilon}_{\pm}$ for the fields $\mathbf{u}^{\varepsilon}$ and $\boldsymbol{\sigma}^{\varepsilon}$ lead to matching relationships between external and internal expansions [23, 25]. In terms of displacements the following relationship have to be satisfied:

$$\mathbf{u}^{\varepsilon}(\mathbf{x}_{\alpha}, \pm\frac{\varepsilon}{2}) = \hat{\mathbf{u}}^{\varepsilon}(\mathbf{z}_{\alpha}, \pm\frac{1}{2}) = \bar{\mathbf{u}}^{\varepsilon}(\mathbf{z}_{\alpha}, \pm\frac{1}{2}) \tag{A.24}$$

where $\mathbf{x}_{\alpha} := (x_1, x_2)$, $\mathbf{z}_{\alpha} := (z_1, z_2) \in \mathcal{S}$. Expanding the displacement in the adherents $\mathbf{u}^{\varepsilon}$, in Taylor series along the x_3-direction and taking into account Eq. (A.5a), it results:

$$\begin{aligned} \mathbf{u}^{\varepsilon}(\mathbf{x}_{\alpha}, \pm\frac{\varepsilon}{2}) &= \mathbf{u}^{\varepsilon}(\mathbf{x}_{\alpha}, 0^{\pm}) \pm \frac{\varepsilon}{2}\mathbf{u}^{\varepsilon}_{,3}(\mathbf{x}_{\alpha}, 0^{\pm}) + \cdots \\ &= \mathbf{u}^{0}(\mathbf{x}_{\alpha}, 0^{\pm}) + \varepsilon\mathbf{u}^{1}(\mathbf{x}_{\alpha}, 0^{\pm}) \pm \frac{\varepsilon}{2}\mathbf{u}^{0}_{,3}(\mathbf{x}_{\alpha}, 0^{\pm}) + \cdots \end{aligned} \tag{A.25}$$

Substituting Eqs. (A.5b) and (A.5c) together with Eq. (A.25) in Eq. (A.24), it holds true:

$$\begin{aligned} &\mathbf{u}^{0}(\mathbf{x}_{\alpha}, 0^{\pm}) + \\ &+\varepsilon\mathbf{u}^{1}(\mathbf{x}_{\alpha}, 0^{\pm}) \pm \frac{\varepsilon}{2}\mathbf{u}^{0}_{,3}(\mathbf{x}_{\alpha}, 0^{\pm}) + \cdots = \hat{\mathbf{u}}^{0}(\mathbf{z}_{\alpha}, \pm\frac{1}{2}) + \varepsilon\hat{\mathbf{u}}^{1}(\mathbf{z}_{\alpha}, \pm\frac{1}{2}) + \cdots \\ &\qquad = \bar{\mathbf{u}}^{0}(\mathbf{z}_{\alpha}, \pm\frac{1}{2}) + \varepsilon\bar{\mathbf{u}}^{1}(\mathbf{z}_{\alpha}, \pm\frac{1}{2}) + \cdots \end{aligned} \tag{A.26}$$

By identifying the terms in the same powers of ε, Eq. (A.26) gives:

$$\mathbf{u}^{0}(\mathbf{x}_{\alpha}, 0^{\pm}) = \hat{\mathbf{u}}^{0}(\mathbf{z}_{\alpha}, \pm\frac{1}{2}) = \bar{\mathbf{u}}^{0}(\mathbf{z}_{\alpha}, \pm\frac{1}{2}) \tag{A.27}$$

$$\mathbf{u}^{1}(\mathbf{x}_{\alpha}, 0^{\pm}) \pm \frac{1}{2}\mathbf{u}^{0}_{,3}(\mathbf{x}_{\alpha}, 0^{\pm}) = \hat{\mathbf{u}}^{1}(\mathbf{z}_{\alpha}, \pm\frac{1}{2}) = \bar{\mathbf{u}}^{1}(\mathbf{z}_{\alpha}, \pm\frac{1}{2}) \tag{A.28}$$

By identification process, analogous results are obtained in terms of stresses [23, 25]:

$$\sigma^{0}_{i3}(\mathbf{x}_{\alpha}, 0^{\pm}) = \hat{\sigma}^{0}_{i3}(\mathbf{z}_{\alpha}, \pm\frac{1}{2}) = \bar{\sigma}^{0}_{i3}(\mathbf{z}_{\alpha}, \pm\frac{1}{2}) \tag{A.29}$$

$$\sigma^1_{i3}(\mathbf{x}_\alpha, 0^\pm) \pm \frac{1}{2}\sigma^0_{i3,3}(\mathbf{x}_\alpha, 0^\pm) = \hat{\sigma}^1_{i3}(\mathbf{z}_\alpha, \pm\frac{1}{2}) = \bar{\sigma}^1_{i3}(\mathbf{z}_\alpha, \pm\frac{1}{2}) \tag{A.30}$$

for $i = 1, 2, 3$.

A.5. Constitutive equations

The constitutive laws in linear elasticity for the adherents and the interphase are considered:

$$\bar{\boldsymbol{\sigma}}^\varepsilon = \mathbb{A}_\pm(\mathbf{e}(\bar{\mathbf{u}}^\varepsilon)) \tag{A.31a}$$

$$\hat{\boldsymbol{\sigma}}^\varepsilon = \mathbb{B}^\varepsilon(\mathbf{e}(\hat{\mathbf{u}}^\varepsilon)) \tag{A.31b}$$

where $\mathbb{A}_\pm, \mathbb{B}^\varepsilon$ are the elasticity tensor of adherents and of interphase, respectively.

Funding: This work has been supported by the University of Ferrara via FAR grants 2020 and 2021.

References

[1] Sekiguchi, Y., Sato, C. (2021) *Experimental investigation of the effects of adhesive thickness on the fracture behavior of structural acrylic adhesive joints under various loading rates*, Int. J. Adhes. Adhes., 105:102782.

[2] Miao, C., Fernando, D., Heitzmann, M. T., Bailleres, H. (2019) *GFRP-to-timber bonded joints: Adhesive selection*, Int. J. Adhes. Adhes., 94:29-39.

[3] Yamamoto, A., Yoshida, T., Tsubota, K., Takamizawa, T., Kurokawa, H., Miyazaki, M. (2006) *Orthodontic bracket bonding: enamel bond strength vs time*, Am. J. Orthod. Dentofacial Orth., 130(4):435-e1.

[4] Benveniste, Y. and Miloh, T. (2001) *Imperfect soft and stiff interfaces in two-dimensional elasticity*, Mech. Mat., 33 (6):309–323

[5] Hashin, Z. (2002) *Thin interphase/imperfect interface in elasticity with application to coated fiber composites*, J. Mech. Phys. Solid, 50(12):2509-2537.

[6] Frémond, M. (1987) *Adhesion of solids*, J. Mech. Th. Appl., 6(3):383–407.

[7] Bonetti E., Bonfanti G., Lebon F., Rizzoni, R. (2017) *A model of imperfect interface with damage*, Meccanica, 52(8):1911–1922

[8] Raous, M., Cangemi, L., Cocu, M. (1999) *A consistent model coupling adhesion,friction, and unilateral contact*, Comput. Meth. Appl. Mech. Eng., 177(3-4):383–399.

[9] Del Piero, G., Raous, M. (2010) *A unified model for adhesive interfaces with damage, viscosity, and friction*, Eur. J.Mech.-A/Solid, 29(4):496–507.

[10] Freddi, F., Frémond, M. (2006) *Damage in domains and interfaces: a coupled predictive theory*, J. Mech. Mat. Struct., 1(7):1205-1233.

[11] Raffa, M.L., Lebon, F., Rizzoni R. (2016) *On modelling brick/mortar*

interface via a St. Venant-Kirchhoff orthotropic soft interface. Part I: theory, Int. J. Masonry Res. Innov., 1 (2):142-164.

[12] Dumont, S., Lebon, F., Raffa, M. L., Rizzoni, R. (2017) *Towards nonlinear imperfect interface models including micro-cracks and smooth roughness*, Annal Solid Struct. Mech., 9(1-2):13–27.

[13] Raffa, M.L., Lebon, F., Rizzoni R. (2017) *On modelling brick/mortar interface via a St. Venant-Kirchhoff orthotropic soft interface. Part II: in silico analysis*, Int. J. Masonry Res. Innov., 2(4):259-273.

[14] Raffa, M. L., Lebon, F., Rizzoni, R. (2018) *Derivation of a model of imperfect interface with finite strains and damage by asymptotic techniques: an application to masonry structures*, Meccanica, 53(7):1645-1660.

[15] Maurel-Pantel, A., Lamberti, M., Raffa, M. L., Suarez, C., Ascione, F., Lebon, F. (2020) *Modelling of a GFRP adhesive connection by an imperfect soft interface model with initial damage*, Comp. Struct., 239:112034.

[16] Needleman, A. (1990) *An analysis of tensile decohesion along an interface*, J. Mech. Phys. Solids, 38(3):289-324.

[17] Costanzo, F. (1998) *A continuum theory of cohesive zone models: deformation and constitutive equations*, Int. J. Engng. Sci., 36(15):1763-1792.

[18] Alfano G., Sacco E. (2006) *Combining interface damage and friction in a cohesive-zone model*, Int. J. Numer. Meth. Engng. 68 (5):542–582

[19] Chen, P., Chen, S., Peng, J. (2016) *Interface behavior of a thin-film*

bonded to a graded layer coated elastic half-plane, Int. J. Mech. Sci. 115:489-500.

[20] Chen, P., Peng, J., Chen, Z., Peng, G. (2019) *On the interfacial behavior of a piezoelectric actuator bonded to a homogeneous half plane with an arbitrarily varying graded coating*, Eng. Fract. Mech. 220:106647.

[21] Guo, W., Chen, P., Yu, L., Peng, G., Zhao, Y., Gao, F. (2020) *Numerical analysis of the strength and interfacial behaviour of adhesively bonded joints with varying bondline thicknesses*, Int. J. Adhes. Adhes. 98:102553.

[22] Chen, P., Chen, S., Liu, H., Peng, J., Gao, F. (2020) *The interface behavior of multiple piezoelectric films attaching to a finite-thickness gradient substrate* J. Appl. Mech.-Trans. ASME, 87(1):011003.

[23] Lebon, F., Rizzoni, R. (2010) *Asymptotic analysis of a thin interface: The case involving similar rigidity*, Int. J. Engng. Sci., 48:473–486

[24] Lebon, F., Rizzoni, R. (2011) *Asymptotic behavior of a hard thin linear elastic interphase: An energy approach*, Int. J. Solid Struct., 48:441–449

[25] Rizzoni, R., Dumont, S., Lebon, F., Sacco, S. (2014) *Higher order model for soft and hard interfaces*, Int. J. Solid Struct., 51:4137-4148

[26] Dumont, S., Rizzoni, R., Lebon, F., Sacco, E. (2018) *Soft and hard interface models for bonded elements*, Comp. Part B: Engng., 153:480–490.

[27] Furtsev, A., Rudoy, E. (2020) *Variational approach to modelling soft*

and stiff interfaces in the Kirchhoff-Love theory of plates*, Int. J. Solid Struct., 202:562–574.

[28] Rudoy, E., Shcherbakov, V. (2020) *First-order shape derivative of the energy for elastic plates with rigid inclusions and interfacial cracks*, Appl. Math. Optim., 1-28.

[29] Baranova, S., Mogilevskaya, S. G., Nguyen, T. H., Schillinger, D. (2020) *Higher-order imperfect interface modelling via complex variables based asymptotic analysis*, Int. J. Engng. Sci., 157:103399.

[30] Raffa, M.L., Lebon, F., Vairo, G. (2016) *Normal and tangential stiffnesses of rough surfaces in contact via an imperfect interface model*, Int. J. Solid Struct., 87:245-253.

[31] Raffa, M. L., Rizzoni, R., Lebon, F. (2021) *A Model of Damage for Brittle and Ductile Adhesives in Glued Butt Joints*, Technologies, 9(1):19.

[32] Kachanov, M., (1994) *Elastic solids with many cracks and related problems*, Adv. Appl. Mech., 30:259-445.

[33] Mauge C., Kachanov M. (1994) *Effective elastic properties of an anisotropic material with arbitrarily oriented interacting cracks*, J. Mech. Phys. Solid, 42:561–584.

[34] Tsukrov, I., Kachanov M. (2000) *Effective moduli of an anisotropic material with elliptical holes of arbitrary orientational distribution*, Int. J. Solid Struct., 37 (41):5919-5941.

[35] Kachanov, M., Sevostianov, I. (2005) *On quantitative characterization of microstructures and effective properties*, Int. J. Solid Struct., 42(2):309-336.

[36] Sevostianov, I., Kachanov, M. (2014) *On some controversial issues in effective field approaches to the problem of the overall elastic properties*, Mech. Mat., 69:93-105.

[37] Kachanov, M., Sevostianov, I. (2018) *Micromechanics of materials, with applications*, (Vol. 249), Cham: Springer.

[38] Bruno, G., Kachanov, M., Sevostianov, I., Shyam, A. (2019) *Micromechanical modelling of non-linear stress-strain behavior of polycrystalline microcracked materials under tension*, Acta Materialia, 164:50-59.

[39] Andrieux, S., Bamberger, Y., Marigo, J. J. (1986) *Un modèle de matériau microfissuré pour les bétons et les roches*, J. Méc. Théor. Appl, 5(3)47:1-513.

[40] Welemane, H., Goidescu, C. (2010) *Isotropic brittle damage and unilateral effect*, Compte Rendu Mec., 338(5):271-276.

[41] Sanchez-Palencia, E. (1980) *Non homogeneous materials and vibration theory*, Lecture Notes in Physics, Springer, Berlin, 127.

[42] Hubert, J. S., Palencia, E. S. (1992) *Introduction aux méthodes asymptotiques et à l'homogénéisation: application à la mécanique des milieux continus*, Masson.

[43] Klarbring A. (1991) *Derivation of the adhesively bonded joints by the asymptotic expansion method*, Int. J. Engng. Sci., 29:493–512.

[44] Geymonat, G., Krasucki, F., Lenci, S. (1999) *Mathematical analysis of a bonded joint with a soft thin adhesive*, Math. Mech. Solid, 10:201–225.

[45] Schmidt, P. (2008) *Modelling of adhesively bonded joints by an asymptotic method*, Int. J. Engng. Sci., 46(12):1291-1324.

[46] Ciarlet P.G. (1988) *Mathematical Elasticity. Volume I: Three-Dimensional Elasticity*, North-Holland, Amsterdam.

[47] Serpilli, M., Lenci, S. (2008) *Limit models in the analysis of three different layered elastic strips*, Eur. J.Mech.-A/Solid, 27(2):247-268.

[48] Serpilli, M., Lenci, S. (2016) *An overview of different asymptotic models for anisotropic three-layer plates with soft adhesive*, Int. J. Solid Struct., 81:130-140.

[49] Goidescu, C., Welemane, H., Kondo, D., Gruescu, C. (2013) *Microcracks closure effects in initially orthotropic materials*, Eur. J.Mech.-A/Solid, 37:172-184.

[50] Goidescu, C., Welemane, H., Pantalé, O., Karama, M., Kondo, D. (2015) *Anisotropic unilateral damage with initial orthotropy: A micromechanics-based approach*, Int. J. Damage Mech., 24(3):313-337.

[51] Eshelby, J. D. (1961) *Progress in solid mechanics*, J. Mech. Phys. Solid, 9(1):67-67.

[52] Welemane, H., Cormery, F. (2002) *Some remarks on the damage unilateral effect modelling for microcracked materials*, Int. J. Damage Mech., 11(1):65-86.

[53] Frémond, M., Nedjar, B. (1996) *Damage, gradient of damage and principle of virtual power*, Int. J. Solid Struct., 33(8):1083-1103.

[54] Chaboche, J. L. (1988) *Continuum damage mechanics: Part I—General concepts*, J. Appl. Mech., 55:59-64.

[55] Wolfram Research, Inc. *Mathematica*; Version 12.2; Wolfram Research, Inc.: Champaign, IL, USA, 2020.

[56] Murakami, S., Sekiguchi, Y., Sato, C., Yokoi, E., Furusawa, T. (2016) *Strength of cylindrical butt joints bonded with epoxy adhesives under combined static or high-rate loading*, Int. J. Adhes. Adhes., 67:86–93.